ACS Catalysis

Research Article

pubs.acs.org/acscatalysis

Mechanistic Aspects of the Water−Gas Shift Reaction on Isolated and Clustered Au Atoms on CeO_2(110): A Density Functional Theory Study

Weiyu Song and Emiel J. M. Hensen*

Laboratory of Inorganic Materials Chemistry, Schuit Institute of Catalysis, Eindhoven University of Technology, P.O. Box 513, 5600 MB Eindhoven, The Netherlands

ABSTRACT: Density functional theory was employed to study the water−gas shift (WGS) reaction for two structural models—namely, a single Au atom and a Au nanorod—supported on the (110) surface of ceria. The carboxyl mechanism involving a COOH intermediate is strongly preferred over the redox mechanism, which would require O−H bond cleavage of ceria-bound hydroxyl groups. Two candidate rate-controlling elementary reaction steps were identified in the carboxyl mechanism: oxygen vacancy formation and COOH formation from CO and OH adsorbed to Au and the ceria support, respectively. A reaction energy analysis shows that both steps are more favorable on clustered Au atoms than on a single Au atom. CO adsorption on a single Au atom is hindered because of its negative charge. Comparison to literature data shows that the WGS reaction is preferred for a gold cluster on the CeO_2(110) surface over the CeO_2(111) one because of the lower binding energy of OH on the former surface. These results are discussed in the light of a large number of experimental and theoretical studies of the Au/CeO_2 catalyzed WGS reaction.

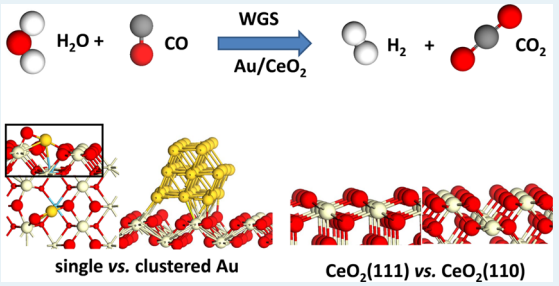

KEYWORDS: *density functional theory, Au/CeO_2, WGS, active site, reaction mechanism, structure sensitivity*

1. INTRODUCTION

The water−gas shift (WGS) reaction is industrially important for the upgrading of hydrocarbon-based fuel reformate streams. Because this reaction is limited by the WGS equilibrium at typical reaction temperatures, it has become customary to carry out the WGS reaction at the industrial scale in two stages: one at higher temperature, typically with iron, and the other one at lower temperature with copper as the main catalytic metal. However, for generation of CO-free H_2, as, for instance, required for PEM fuel cell applications, the activity of these commercial catalysts is too low.[1−3] In the past decade, metal-oxide-supported gold nanoparticle catalysts have been explored as potential WGS catalysts.[1−3]

Despite intensive research, the nature of the catalytically active gold species under WGS reaction conditions (single site Au atoms vs clustered Au atoms; ionic vs metallic) remains strongly debated.[1−3] Fu et al.[4] found that the WGS rate for Au/CeO_2 was not affected by cyanide leaching of metallic Au nanoparticles and asserted that atomically dispersed Au cations instead of nanocrystalline gold catalyzes the WGS reaction. Recently, Yang et al.[5] employed UV treatment to stabilize isolated gold atoms on TiO_2 and contended that these catalyze the WGS reaction at low temperature. For Au/Fe_2O_3, Allard et al.[6,7] showed that atomic gold species are strongly bound to the support, even after redox heat treatments and exposure to the WGS reaction conditions.

In contrast to these studies, other experimental works provide compelling evidence for the opposite conclusion, namely, that the WGS reaction is catalyzed by metallic Au clusters or nanoparticles. Kim et al.[8] performed a leaching procedure similar to that of Fu et al. and found that the reaction rate before leaching was significantly higher than after leaching. On this basis, they argued that nanocrystalline gold plays an important role in the WGS reaction. A similar conclusion was reached by Behm's group.[9] Previous experimental work from our group showed that the cationic gold in leached Au/CeO_2 will (partially) reduce and form very small metallic gold clusters active for the hydrogenation of 1,3-butadiene, CO oxidation, and the WGS reaction.[10,11] Rodriguez and co-workers studied Au/Ce(Gd)O_2 and Au/CeO_x/TiO_2 by in situ time-resolved X-ray absorption spectroscopy[12,13] and observed transformation of cationic gold to metallic gold under WGS conditions.

Au/TiO_2 prepared by a deposition-precipitation technique of gold was recently investigated for the WGS reaction.[14,15] On the basis of kinetic data and geometric arguments, it was proposed that the corner atoms on the gold cuboctahedron nanoparticles with fewer than seven neighboring gold atoms are the dominant active sites. The total rate is proportional to the number of gold particles, yet it does not depend on their size. This view was recently further supported by halide poisoning of the active sites.[16]

Received: December 17, 2013
Revised: April 26, 2014
Published: May 1, 2014

   dx.doi.org/10.1021/cs401206e | ACS Catal. 2014, 4, 1885−1892

Three main mechanisms have been proposed for the WGS reaction: redox, formate, and carboxyl mechanisms. It is well-known that the ceria support itself exhibits the ability to store and release oxygen under oxidizing and reducing conditions. On the basis of this, Flytzani-Stephanopoulos and co-workers prefer to describe reactivity of Au/CeO_2 in terms of the redox mechanism with CO being adsorbed to gold and oxidized by an O atom of ceria, followed by reoxidation of the support by water to give hydrogen.[4] The formate mechanism was first proposed by Shido and Iwasawa and involves the reaction of CO with surface OH groups to form the HCOO group intermediate.[17,18] On the basis of spectroscopic investigations, several groups have provided further support for this mechanism.[9,19] However, Meunier et al.[20] investigated the WGS activity of $Au/Ce(La)O_2$ by operando diffuse reflectance infrared Fourier transform spectroscopy and found that the rate of formate decomposition was 60-fold smaller than the rate of CO_2 formation, pointing to the minor role of surface formate in the reaction mechanism. Accordingly, it may be expected that formate is a spectrator species.

As an alternative, Buch proposed the carboxyl mechanism,[2] although no clear experimental evidence for involvement of the COOH intermediate in the WGS reaction has been presented yet. The carboxyl mechanism was explored using theoretical methods by several groups. On the basis of a $Au_4/CeO_{2-x}(111)$ model, Liu et al.[21] proposed the dissociation of H_2O to adsorbed H and OH; CO reaction with OH to give adsorbed COOH; COOH dissociation to give CO_2 and adsorbed H; and finally, recombination of the two H atoms on Au to form H_2. Rodriguez et al. explored the same mechanism on a larger Au_{29} cluster.[22] Water dissociation was found to be the rate-limiting step, and the authors suggested that a reduced ceria support facilities H_2O dissociation. Following this line, the authors performed extensive work on oxide supported metals to show the importance of the metal−support interface in the WGS reaction.[23] It is worth mentioning that for Cu(111), Gokhale et al. explored the same mechanism, except for the COOH dissociation step: instead of direct dissociation of H to the Cu surface, COOH dissociates its H to form an OH surface intermediate.[24] A similar dissociation step was studied by Liu et al. for Au(111).[25]

On the basis of a $Au_n/CeO_2(111)$ model, Chen et al. compared redox and formate mechanisms.[26] They found that it is energetically unfavorable to break the O−H bond of the ceria-adsorbed OH group, which is a key step in both mechanisms. Their following work proposed a feasible alternative carboxyl mechanism.[27] From the above, we conclude that the mechanisms essentially can be divided into two groups: one involves OH bond cleavage (redox and formate mechanisms); the other one involves OH reacting with CO to form COOH (carboxyl mechanism). Considering the similarity between redox and formate mechanisms in the key step of OH bond cleavage, we will focus in the present study on the redox mechanism and compare it with the carboxyl mechanism to identify the dominant reaction path under low temperature conditions.

The influence of the ceria surface termination of Au/CeO_2 catalysts on the WGS performance has been reported in several experimental works.[10,28] To this purpose, gold-ceria catalysts are typically prepared by depositing gold on the surface of ceria nanorods, nanocubes, or polyhedra. The WGS activity strongly depends on the crystal plane of the CeO_2. Ceria powder catalyst mainly exposes the {111} surface. Rodlike ceria enclosed by {110} and {100} planes were found to be the most active for gold stabilization/activation. Similar synergistic effects have been reported for such reactions as CO oxidation,[29] CO_2 reforming of methane,[30] methanol and ethanol reforming,[31] and soot oxidation.[32] Theoretical studies[33−35] suggest that the more open nature of the surface of $CeO_2(110)$ provides a good explanation for the high CO oxidation activity. To the best of our knowledge, no systematic theoretical study has been carried out on the effect of ceria surface termination on the Au/CeO_2-catalyzed WGS reaction. Accordingly, in the present work, we investigate the WGS reaction mechanism for two structural models of gold, namely, a single Au atom and a Au cluster, both supported on $CeO_2(110)$ with the aim of understanding (i) the active site (atomically dispersed Au vs metallic Au cluster), (ii) the dominant reaction mechanism at low reaction temperatures (redox vs carboxyl), and (iii) the influence of ceria surface termination. For the latter purpose, we carried out additional calculations using a Au_3 cluster on the defective $CeO_2(110)$ surface and compare our results to data reported for Au supported on the $CeO_2(111)$ surface.[21,26,27]

2. COMPUTATIONAL DETAILS

Density functional theory (DFT) with the PBE (Perdew−Burke−Ernzerhof) functional[36] as implemented in the Vienna Ab Initio Simulation Package[37−39] was employed. A Hubbard U term was added to the PBE functional (DFT+U) employing the rotationally invariant formalism by Dudarev et al.,[40] in which only the difference ($U_{eff} = U - J$) between the Coulomb U and exchange J parameters enters. Spin-polarized calculations were performed. The projector augmented wave method[41−43] was used to describe the interaction between the ions and the electrons with the frozen-core approximation.[41] The valence electrons were treated using a plane-wave basis set with a kinetic energy cutoff of 400 eV.

For Ce, a value of U_{eff} = 4.5 eV was used, which was calculated self-consistently by Fabris et al.[44] using the linear response approach of Cococcioni and De Gironcoli.[45] This value is within the 3.0−5.5 eV range reported to provide localization of the electrons left upon oxygen removal from CeO_2.[46] For single Au on $CeO_2(110)$ model, a 2 × 3 cell was used. The Au atom was placed on the clean surface of $CeO_2(110)$. Another relevant state of this Au atom is on an oxygen vacancy site of the defective $CeO_2(110)$ surface. The alternative location of the gold atom on a Ce vacancy was not considered here because a previous theoretical study suggests that it is not stable.[47] For the Au nanorod on $CeO_2(110)$, a 3 × 3 cell was used for $CeO_2(110)$.

Due to the large size of the surface cells for both models, a 1 × 1 × 1 k-point mesh was used for the Brillouin zone integration. The bulk equilibrium lattice constant (5.49 Å) previously calculated by PBE+U (U_{eff} = 4.5 eV) was used.[48] The slab was five layers thick, and the vacuum gap was set to 25 Å. The three top atomic layers of the ceria slab were allowed to relax while the bottom two layers were kept fixed to their bulk positions. Atoms were relaxed until forces were smaller than 0.05 eV·Å^{-1}.

The location and energy of transition states were calculated with the climbing-image nudged elastic band method.[49] All transition states were verified by the existence of a single imaginary frequency along the reaction coordinate. For the Au nanorod model, all of the Au atoms were allowed to relax in the y- and z-directions. This model has been employed before by several groups to identify plausible reaction mechanisms and

dx.doi.org/10.1021/cs401206e | ACS Catal. 2014, 4, 1885−1892

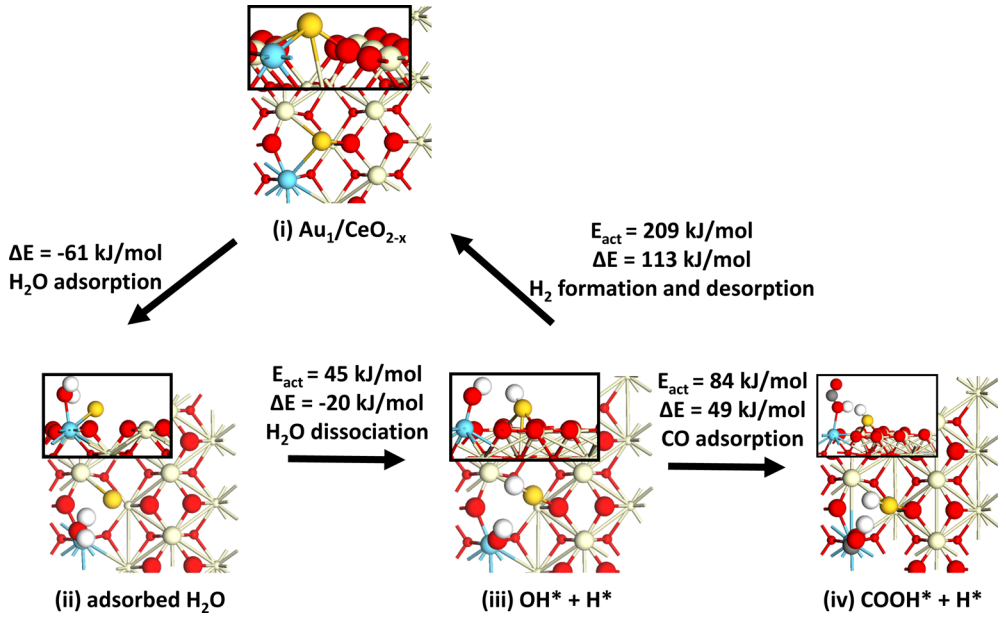

Figure 1. Elementary reaction steps in the WGS reaction on $Au_1/CeO_2(110)$. For the ceria surface slab, only the top two layers are shown with the second layer in small spheres. Color scheme: red (oxygen), white (cerium), bright white (hydrogen), yellow (gold), green (reduced cerium), and black (carbon).

identify active sites to represent supported Au particles.[50] The benefit of this model is that the Au nanorod structure is computationally tractable and represents the interface between Au nanoparticles and the support. For the models containing an isolated Au atom and a cluster of 3 Au atoms, the metal phase was allowed to relax in all three directions.

3. RESULTS AND DISCUSSION

The reaction mechanism for the WGS reaction for a $CeO_2(110)$-supported single Au (denoted as $Au_1/CeO_2(110)$ throughout this paper) and a $CeO_2(110)$ supported Au nanorod (denoted as $Au_n/CeO_2(110)$) will be explored extensively in sections 3.1 and 3.2, respectively. In section 3.3, we will compare the results for these two different models and also discuss the influence of surface termination of the ceria surface, that is, $CeO_2(110)$ vs $CeO_2(111)$. For the latter purpose, we also repeat the energy analysis of the most important reaction steps for a Au_3 model.

3.1. WGS Reaction on $Au_1/CeO_2(110)$. As follows from our recent work,[33] a single Au atom prefers to adsorb onto the bridge site between two surface O atoms on $CeO_2(110)$. One of these surface O atoms spontaneously migrates to the bridge site between Ce and Au, generating a highly reactive Au−O_s species, which may be easily reduced by CO. This will generate a surface oxygen vacancy neighboring Au. Such oxygen vacancies may play an important role in the water activation step at the interface between the Au adatom and ceria surface.[23,27] Thus, we start our exploration of the WGS mechanism from this defective $Au_1/CeO_{2-x}(110)$ surface.

The relevant elementary reaction steps and the involved energy changes are shown in Figure 1. Water adsorbs at the interface between Au and the defective ceria surface with an energy of 61 kJ/mol. This value is comparable to previously reported adsorption energies for water on defective ceria surfaces (82 kJ/mol[27] and 62 kJ/mol[51]). Water dissociation proceeds with a barrier of 45 kJ/mol to produce a H atom on the Au atom and an OH group attached to the Ce^{3+} site from the ceria support (state iii, Figure 1). This reaction is exothermic by 20 kJ/mol. The redox mechanism for H_2 formation involves the reaction of ceria-bound OH with Au-bound H to give H_2. The barrier for this step is 209 kJ/mol, with a positive reaction energy of 113 kJ/mol. On $Au_n/CeO_2(111)$,[26] the reaction energy for the H_2 formation step was reported to be between 108 and 134 kJ/mol. The reason for the high barrier of this step is the strong O−H bond energy. The same argument was put forward by Hu and co-workers[26] to explain the unfavorable energetics for CO inserting into the OH group to form HCOO (formate mechanism). This reaction also involves O−H bond cleavage. The proposed high strength of the O−H bond is consistent with the experimental observations of Rodriguez and colleagues.[52] Water was adsorbed onto a $CeO_{1.75}/Au(111)$ surface at 100 K, followed by thermal annealing. The OH species are stable on the surface up to 600 K. The high barrier for H_2 formation suggests that the redox mechanism is relevant only at high temperatures, supporting speculations based on experiment.[2] To sum up, the strong O−H bound makes the direct redox mechanism difficult at low temperatures. The same applies to the formate mechanism because it also requires O−H bond cleavage,[26] which was therefore not explored further herein.

The alternative carboxyl mechanism in which the ceria-adsorbed OH group reacts with CO was also examined for the $Au_1/CeO_2(110)$ model; however, no CO adsorption state could be identified for the isolated Au atom (state iii, Figure 1). This result can be understood from the negative charge state of the single Au adatom, which has been discussed in detail in our previous work.[33] The higher the negative charge on the Au atom is, the weaker the bond energy with CO (repulsion with the 5σ HOMO of CO). Alternatively, the Eley−Rideal mechanism in which CO from the gas phase directly reacts with the surface OH group to form COOH was examined. It turns out the barrier for this step is 84 kJ/mol, with the final state being less stable by 49 kJ/mol than the initial one. If we take into consideration the effect of entropy loss for this

dx.doi.org/10.1021/cs401206e | ACS Catal. 2014, 4, 1885−1892

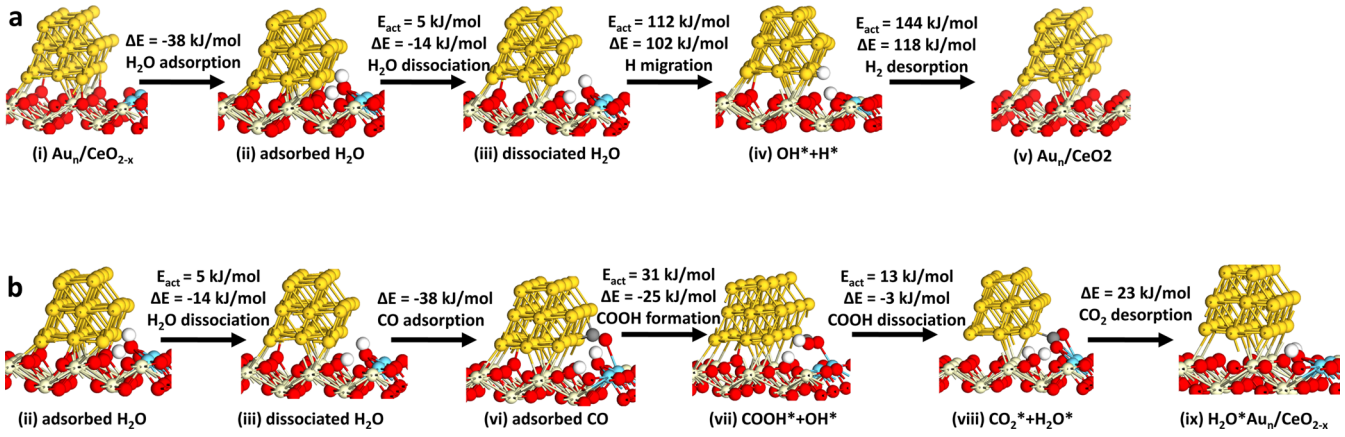

Figure 2. Reaction scheme of (a) the redox mechanism and (b) the first part of the carboxyl path for the WGS reaction on the $Au_n/CeO_2(110)$ model.

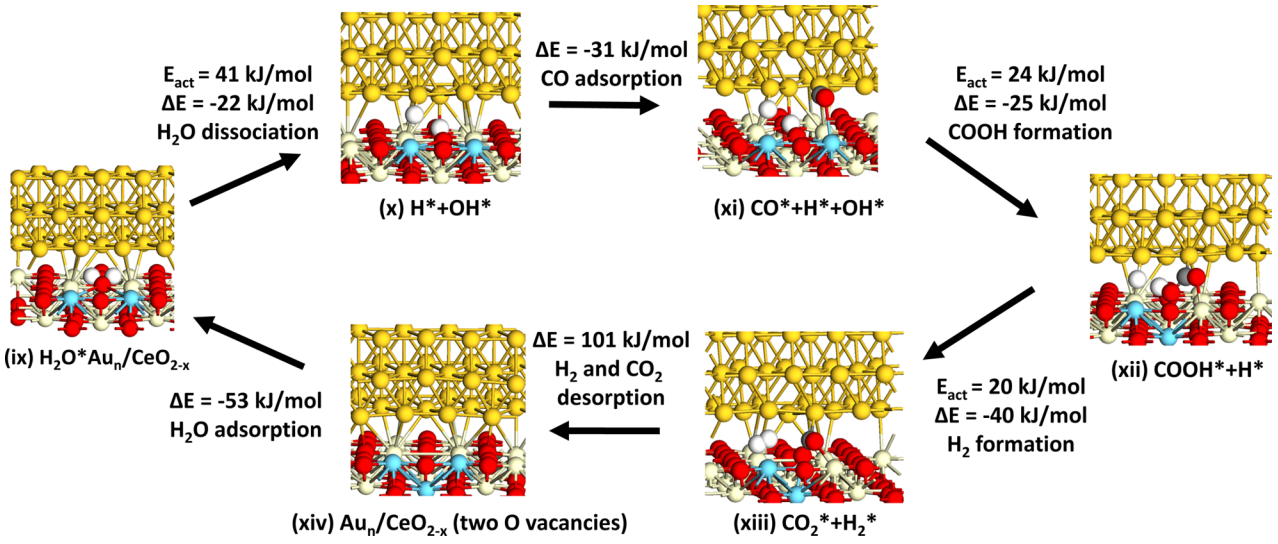

Figure 3. Reaction scheme of the catalytic cycle of carboxyl pathway for the WGS reaction on the $Au_n/CeO_2(110)$ model.

mechanism starting from CO in the gas phase, the free energy barrier for this process would be much larger than this value. For example, taking into account the entropy of the CO at room temperature (196.67 J/mol.K, T = 298 K), we predict an overall barrier for this process of 143 kJ/mol. On this basis, we exclude the possibility for this mechanism to the WGS reaction at low temperatures.

Thus, for the $Au_1/CeO_2(110)$ model, the redox mechanism will be relevant only to the overall reaction rate at relatively high temperatures because of the strong O−H bond of the hydroxyl bound to ceria. This prevents recombinative H_2 formation with the H atom adsorbed to the single Au atom. The same reasoning applies to the formate mechanism. Because a single Au atom cannot adsorb CO as a result of its support interaction induced negative charge, we predict that the WGS reaction will also not proceed via the carboxyl mechanism for isolated Au atoms at low temperatures. Although, in principle, such isolated Au atoms may be involved in the WGS reaction at high reaction temperatures, one has to keep in mind that typically, isolated Au atoms will sinter under such conditions. For gold on $CeO_2(111)$, sintering of isolated gold atoms has also been explored computationally.[53]

3.2. WGS Reaction on $Au_n/CeO_2(110)$. For the gold nanorod model on the $CeO_2(110)$ surface, we start from CO adsorption at the interface between the gold nanorod and the support surface. This leads to spontaneous reaction of CO with a ceria surface O atom and desorption as CO_2, generating one oxygen vacancy at the interface.[34] Similar to results for the model with an isolated gold atom, we initiate the catalytic cycle from this state. The relevant reactions are depicted in Figures 2 and 3, and the corresponding potential energy diagram is given in Figure 4. Water adsorbs molecularly at the interface between the oxygen vacancy and the Au nanorod with its two H atoms pointing to a surface O atom and the Au nanorod, respectively. The adsorption energy is 38 kJ/mol. It takes only 5 kJ/mol to dissociate one of the OH bonds, forming two hydroxyl groups on the ceria support. The final state is 14 kJ/mol more stable than the adsorbed state of water. Direct formation of H_2 from this state costs a prohibitive energy of 220 kJ/mol. This result is consistent with the difficulty in cleaving O−H bonds in the $Au_1/CeO_2(110)$ model.

An alternative path involves migration of the H of OH to the Au nanorod, followed by reaction with OH on the ceria support. The barrier for H migration is 112 kJ/mol, and it is endothermic by 102 kJ/mol. The migrated H atom is located at the bridge site of two Au atoms. It then reacts with the other OH group of the ceria support to form H_2 with a reaction barrier of 144 kJ/mol and a reaction energy of 118 kJ/mol.

dx.doi.org/10.1021/cs401206e | ACS Catal. 2014, 4, 1885−1892

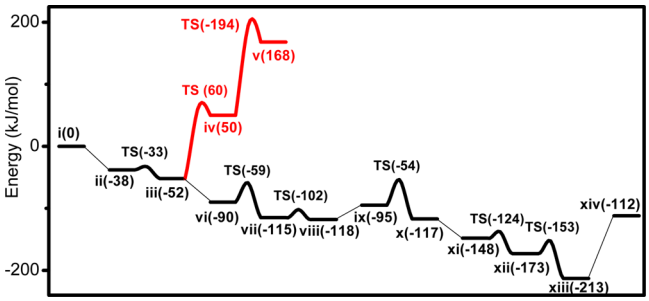

Figure 4. Potential energy diagram for the WGS reaction on $Au_n/CeO_2(110)$. The states with Roman numerals refer to the structures in Figures 2 and 3. The red and black lines represent the redox and carboxyl paths, respectively.

These barriers for H_2 formation are relatively high so that we predict that this pathway would also require relatively high reaction temperatures. An important corollary of these calculations is that the redox mechanism will be important only for WGS reactivity at higher reaction temperatures and that the rate is not expected to depend on the size of the gold phase, that is, single site Au, small Au_3,[26] Au_{10},[26] or large Au clusters would have quite similar barriers for the most difficult step, namely, H_2 formation. Obviously, the rate may be expected to corrolate with the gold dispersion and, more accurately, with the perimeter surface between gold and the ceria support.

Instead of direct OH bond cleavage, we then considered the carboxyl mechanism for the Au nanorod model. In this pathway, CO first adsorbs onto the Au nanorod neighboring the OH group with an adsorption energy of −38 kJ/mol. The reaction proceeds by COOH formation between adsorbed CO and OH fragments. The barrier for this process is 31 kJ/mol, with a favorable exothermic reaction energy of −25 kJ/mol. Two possible paths exist for COOH decomposition. The first one is dissociation of the COOH to CO_2 and H, the former desorbing and the latter moving to the Au nanorod. The barrier for this process is 76 kJ/mol, and the corresponding reaction energy is 11 kJ/mol. The reaction barrier for COOH dissociation is lower than a previously reported value (104 kJ/mol) for a planar Au_4 cluster supported on $CeO_{2-x}(111)$.[21] The difference can be attributed to the lower coordination number of Au in the present work, making it more reactive in this particular step.

A second pathway involves dissociation of the COO−H to the OH group locating at ceria support, thus forming a COOH−OH complex. The barrier for this path is only 13 kJ/mol, significantly lower than the first one. The final state is more stable by 3 kJ/mol than the initial one. This finding is consistent with previous studies on Cu(111),[24] Au(111),[25] and $Au_n/CeO_2(111)$,[27] in which it was found that COOH prefers to dissociate its proton to the OH group instead of the metal surface. It takes 23 kJ/mol to desorb the CO_2 molecule into the gas phase, leaving water on the two surface oxygen vacancies at the interface between the Au cluster and ceria. Water will then dissociate one of its H atoms to the Au cluster, leaving an OH group behind on the ceria support. The barrier for water dissociation is 41 kJ/mol and the reaction energy is −22 kJ/mol. The values are very close to those for the same process on $Au_1/CeO_{2-x}(111)$ (E_{act} = 45 kJ/mol; E_{react} = −20 kJ/mol), in which water dissociates H to Au, leaving behind the OH group on the defective ceria support. The process becomes easier when water dissociates its H to the surface O to form two OH groups on the ceria support (E_{act} = 5 kJ/mol; E_{react} = −14 kJ/mol), as described above.

The reaction continues by adsorption of another CO at the Au nanorod (E_{ads} = 31 kJ/mol). CO will then easily react with this remaining OH group, forming COOH with activation and reaction energies of 24 and −25 kJ/mol, respectively. The H atom of COOH points to the H dissociated from H_2O in the previous step (state xii). These two H atoms form H_2, leaving CO_2 attached to the ceria support. The barrier for this last step is 20 kJ/mol, and the final state is 40 kJ/mol more stable than the initial state. It takes 101 kJ/mol to desorb H_2 and CO_2 into the gas phase.

From state xii, one can imagine another possible reaction path: first, the H atom migrates to another site on the Au cluster, and then COOH dissociates its H atom to the Au nanorod, and CO_2 desorbs into the gas phase. Finally, the two H atoms adsorbed on gold form H_2. As shown above, the barrier for the COOH dissociation step is 76 kJ/mol, which is much larger than the barrier for direct COOH dissociation (E_{act} = 20 kJ/mol). Accordingly, we did not consider this alternative further. After desorption of H_2 and CO_2, two oxygen vacancies are present on the ceria support. Water then adsorbs at the interface site between the Au nanorod and the defective ceria support, closing the catalytic cycle. From the above, we deduce that the reaction cycle proceeds from state ix (water adsorbed at the interface between the defective ceria support with two oxygen vacancies and the Au nanorod) and state xiv (Au nanorod supported on defective ceria support with two oxygen vacancies), shown in Figure 3. Accordingly, we infer that the active site consists of the Au nanorod supported on the defective ceria support with a proximate oxygen vacancy. Earlier, Tabakova et al. used X-ray photoelectron spectroscopy to show that the Ce^{3+} content of the surface layer is ∼30% during the WGS reaction,[54] suggesting that these vacancies are in close contact with the nanosized metallic gold clusters and associated with the high WGS activity. The mechanism explored in the present study supports this speculation.

3.3. General Discussion. A significant debate has arisen in the scientific literature on the nuclearity of the gold phase (single Au atom vs clustered Au atoms) in Au/CeO_2 WGS catalysts.[1−11] The present theoretical study helps to better understand this issue. We distinguish two key elementary steps in the WGS reaction mechanism. The first one is the formation of oxygen vacancies on the ceria surface, which are essential for the activation of water. In our model, oxygen vacancies are generated by reduction with gas phase CO. For the $Au_1/CeO_2(110)$ model, this poses a problem because the Au adatom cannot adsorb CO. An alternative way of removing the surface oxygen is by an Eley−Rideal mechanism (E_{act} = 45 kJ/mol; $E_{reaction}$ = −28 kJ/mol), whose reaction rate is expected to be low. For the $Au_1/CeO_2(111)$ model,[55] CO adsorption is possible when the gold atom is positively charged. The study of Camellone and Fabris showed that upon CO_2 formation and desorption, the Au ion will migrate to the resulting oxygen vacancy site to block site for water activation. Moreover, the Au atom will become negatively charged in this configuration, preventing further CO adsorption. The initiating step in the mechanism will proceed much more easily on the $Au_n/CeO_2(110)$ model because CO will be able to adsorb onto the gold phase, and it will react with negligible barrier with a ceria surface oxygen atom to form CO_2. Thus, for the oxygen

dx.doi.org/10.1021/cs401206e | ACS Catal. 2014, 4, 1885−1892

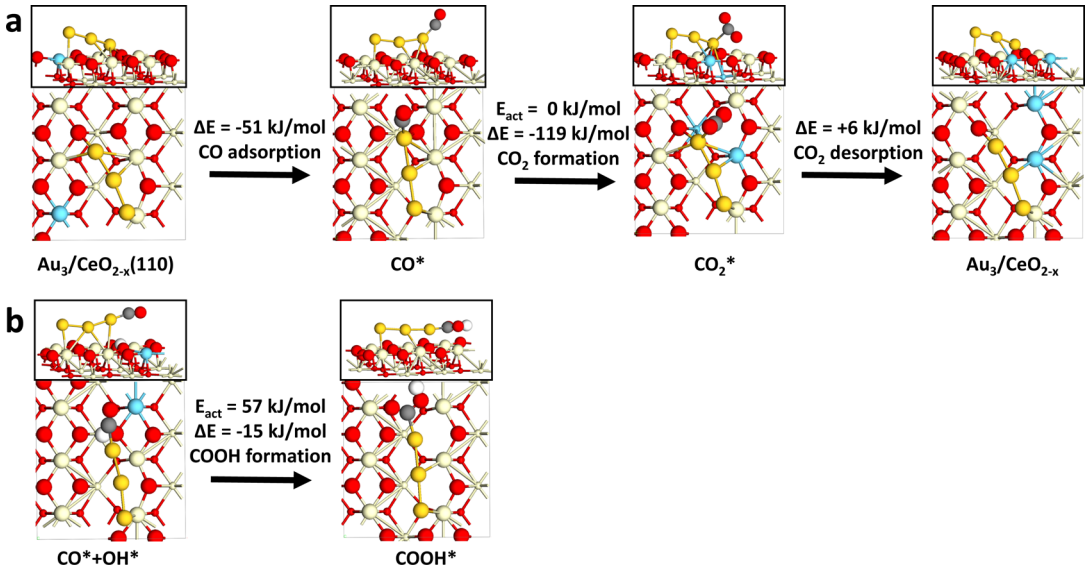

Figure 5. Mechanism and energetics of the oxygen vacancy formation and COOH formation on the $Au_3/CeO_2(110)$ model.

vacancy formation step, gold clusters are expected to be more active than a single gold atom.

The second key step in the WGS reaction is the reaction of CO with OH to form COOH. On the $Au_1/CeO_2(110)$ model, water dissociation leads to one H atom on gold and one in the form of OH on ceria. Similar to the initial $Au_1/CeO_2(110)$ model, no CO adsorption was found on Au after water dissociation. The reaction barrier via the Eley−Rideal mechanism is 84 kJ/mol, and the reaction energy is 49 kJ/mol, implying a low reaction rate at relatively low temperatures. CO can adsorb onto the Au nanorod in $Au_n/CeO_2(110)$ after water dissociation so that the reaction of adsorbed CO will proceed with the OH group of the ceria support. By analyzing the two key steps in WGS, we predict that a Au cluster is much more reactive than a single-site Au atom. In essence, this difference is related to the charge state of a single Au atom. It precludes CO adsorption, which is a prerequisite for both oxygen vacancy formation and COOH formation.

The current proposed mechanisms for WGS can be categorized into two groups: one involving O−H bound cleavage (redox mechanism and formate mechanism), the other one involving COOH as an intermediate (carboxyl). Alternatively, OH reacts with CO to form COOH. In the present contribution, we considered the redox mechanism as representative for the first type. All of the relevant computational studies predict a high barrier for the OH* + H* step to form H_2, which is the key step in the redox mechanism: 130 kJ/mol for $Au_3/CeO_2(111)$;[26] 106 kJ/mol for $Au_{10}/CeO_2(111)$;[26] and in the present work, 209 kJ/mol for $Au_1/CeO_2(110)$ and 144 kJ/mol for $Au_n/CeO_2(110)$. In contrast, the barrier for the COOH formation step is typically much lower, that is, 10 kJ/mol for $Au_4/CeO_2(111)$,[21] 62 kJ/mol for $Au_3/CeO_2(111)$,[26] and 31 kJ/mol for $Au_n/CeO_2(110)$. On the basis of these data, we conclude that the dominant reaction path of WGS under low temperature conditions is the carboxyl mechanism.

An essential part of this work is the comparison of two key elementary steps for the WGS reaction: oxygen vacancy formation and COOH formation. By comparing the kinetics of these two steps for different ceria surface terminations, we aimed to contribute to the understanding of experimentally observed reactivity trends as a function of ceria morphology. For a $Au_n/CeO_2(111)$ model, a previous study has shown that the Mars−van Krevelen mechanism in which adsorbed CO reacts with ceria surface O is inhibited by high desorption energy (E_{des} = 122−209 kJ/mol) because of the strong Ce−O bond strength in the $CeO_2(111)$ surface.[56] With the weaker Ce−O bond in $Au_n/CeO_2(110)$, the enthalpy change associated with CO_2 desorption is −3 kJ/mol, generating one oxygen vacancy.[34] Such a vacancy formation mechanism has been observed in several experimental studies.[57,58] The CO oxidation rate strongly depends on the morphology of the ceria support. Thus, we expect that the nature of the ceria surface termination will significantly influence oxygen vacancy formation and, thus, indirectly the water activation step.

The COOH formation step involves reaction of adsorbed CO with ceria surface OH groups. On $Au_n/CeO_2(110)$, the activation barrier for this step is 31 kJ/mol, with a reaction energy of −25 kJ/mol. On $Au_n/CeO_2(111)$,[27] the activation barrier is 63 kJ/mol, with a reaction energy of 27 kJ/mol. The substantial difference in kinetics is consistent with the experimental observation that gold supported on nanorod ceria, which exposes mainly (110) and (100) surfaces, is much more active than gold on polyhedra with mainly (111) and (100) exposed surfaces.[28] The authors explained these differences in terms of oxygen vacancy formation energies. A lower energy for oxygen vacancy formation will lead to more oxygen vacancies and more ionic gold stabilized on the surface. Our results indicate that both the oxygen vacancy formation energy and the OH reactivity contribute to the observed differences in the WGS activity.

Facile oxygen vacancy formation leads to facile water activation and COOH formation. Recently, we also studied CO oxidation on a single Rh atom supported on $CeO_2(111)$ and (110).[35] It was found that the desorption energy of CO_2 formed from CO reacting with ceria surface O is much lower for $Rh/CeO_2(110)$ than for $Rh/CeO_2(111)$. The difference relates to the lower coordination number of surface O in $CeO_2(110)$ compared with $CeO_2(111)$. On the former surface, oxygen is more weakly bound to the surface cerium ions. Consequently, CO_2 can desorb more easily. The same argumentation is useful to explain the different reactivity of surface OH group on different ceria surfaces: the lower the

dx.doi.org/10.1021/cs401206e | ACS Catal. 2014, 4, 1885−1892

coordination number of the OH group to the cerium cation, the higher the reactivity toward CO. The dependence of OH group reactivity toward CO on ceria surface was also observed for a pure ceria support.[59] It is thus reasonable to conclude that it reflects the intrinsic reactivity differences of OH groups on different ceria surface terminations.

The identification of the exposed facets of different ceria morphologies is still under debate.[28−32,60] In Datye's recent work,[60] it was found that ceria nanorods are enclosed mainly by $CeO_2(111)$ surfaces, not by $CeO_2(110)$ terminations, as usually proposed.[28,32] In accordance with this, no significant activity differences between ceria rod and ceria polyhedra were observed. We point out that others observed substantial activity differences between ceria nanorods and polyhedra.[28−32] The work of Trovarelli et al.[32] has shown that the exact termination of ceria nanoparticles may be controlled by the proper choice of synthesis conditions. Our theoretical results predict that Au clusters supported on the $CeO_2(110)$ surface exhibit much higher activity in the WGS reaction than Au clusters on the $CeO_2(111)$ surface.

To verify that the above conclusions are not influenced by the gold nuclearity in the surface model, we carried out additional calculations using a $Au_3/CeO_{2-x}(110)$ model and compared it with literature data available for the $Au_3/CeO_{2-x}(111)$ model.[27,53b] We examined the two key processes in the WGS mechanism, namely, oxygen vacancy generation by CO reduction of the surface and COOH formation (Figure 5). The Au_3 structure resembles that of the structure reported by Fabris et al.[53b] The first step involves reaction of CO adsorbed to gold with a surface O atom to form CO_2, followed by CO_2 desorption. On the $Au_3/CeO_{2-x}(110)$ model, the CO_2 formation step has a negligible barrier, and the reaction energy is −119 kJ/mol. The desorption energy of CO_2 is only 6 kJ/mol. On $Au_3/CeO_{2-x}(111)$,[53b] the kinetics are less favorable, with a barrier of 63 kJ/mol for the CO_2 formation step and an exothermic reaction energy of −17 kJ/mol. Compared with the nearly thermoneutral value for $Au_3/CeO_{2-x}(110)$, the desorption energy of CO_2 is also less favorable at 56 kJ/mol. The difference is, however, less pronounced, as in the comparison between $Au_3/CeO_2(110)$ and $Au_n/CeO_2(111)$, because migration of the Au_3 cluster closer to the oxygen vacancy for the $Au_3/CeO_{2-x}(110)$ stabilizes the final state following CO_2 desorption. Importantly, these results confirm that it will be much easier to form oxygen vacancies in the $Au_3/CeO_{2-x}(110)$ model than in the $Au_3/CeO_{2-x}(111)$ model. This conclusion is essentially similar to what we inferred from the above comparison of the oxygen vacancy formation energetics between $Au_n/CeO_2(110)$ and $Au_{13}/CeO_2(111)$ models. The barrier for the COOH formation step is 57 kJ/mol for $Au/CeO_{2-x}(110)$, with an exothermic reaction energy of 15 kJ/mol. The values reported for $Au_3/CeO_{2-x}(111)$[27] are a barrier of 62 kJ/mol and an endothermic reaction energy of 27 kJ/mol. Accordingly, this comparison of a Au_3 cluster on a $CeO_2(110)$ and $CeO_2(111)$ supports our conclusion that the higher activity of gold on the $CeO_2(110)$ surface compared with gold on the $CeO_2(111)$ surface is due mainly to the easier oxygen vacancy formation on the more open surface.

4. CONCLUSIONS

Density functional theory was employed to study the WGS activity of gold supported on a $CeO_2(110)$ model surface with the aim to identify the active site (single Au atom vs clustered Au) and reaction mechanism (redox vs carboxyl). For both structural models, it was found that the redox mechanism requires high reaction temperatures because it involves direct cleavage of an O−H bond of the ceria hydroxyl groups. In comparison, the carboxyl mechanism presents a low energy pathway toward formation of CO_2 and H_2. Two candidate rate-controlling elementary reaction steps were identified in the WGS reaction: oxygen vacancy formation and COOH formation from CO and OH, respectively, adsorbed to gold and the ceria support. Both steps proceed at a higher rate on clustered Au than on a single site Au atom. The most important reason for this difference is the negative charge of the single Au atom, which inhibits CO adsorption. These two elementary reaction steps were also found to be preferred on $Au_n/CeO_2(110)$ over $Au_n/CeO_2(111)$, essentially because of the lower binding energy of the OH on the more open surface. This provides an explanation for the experimentally observed surface termination dependence of ceria supports for the gold-catalyzed WGS reaction.

AUTHOR INFORMATION

Corresponding Author

*E-mail: e.j.m.hensen@tue.nl.

Notes

The authors declare no competing financial interest.

ACKNOWLEDGMENTS

We acknowledge financial support for this research from ADEM, A Green Deal in Energy Materials of the Ministry of Economic Affairs of The Netherlands (www.adem-innovationlab.nl). Supercomputing facilities were funded by The Netherlands Organization for Scientific Research.

REFERENCES

(1) Flytzani-Stephanopoulos, M.; Gates, B. C. *Annu. Rev. Chem. Biomol. Eng.* **2012**, *3*, 545−574.
(2) Burch, R. *Phys. Chem. Chem. Phys.* **2006**, *8*, 5483−5500.
(3) Tao, F.; Ma, Z. *Phys. Chem. Chem. Phys.* **2013**, *15*, 15260−15270.
(4) Fu, Q.; Saltburg, H.; Flytzani-Stephanopoulos, M. *Science* **2003**, *301*, 935−938.
(5) Yang, M.; Allard, L. F.; Flytzani-Stephanopoulos, M. *J. Am. Chem. Soc.* **2013**, *135*, 3768−3771.
(6) Allard, L. F.; Flytzani-Stephanopoulos, M.; Overbury, S. H. *Microsc. Microanal.* **2010**, *16*, 375−385.
(7) Allard, L. F.; Borisovich, A.; Deng, W.; Si, R.; Flytzani-Stephanopoulos, M.; Overbury, S. H. *J. Electron Microsc.* **2009**, *58*, 199−212.
(8) Kim, C. H.; Thompson, L. T. *J. Catal.* **2006**, *244*, 248−250.
(9) Leppelt, R.; Schumacher, B.; Plzak, V.; Kinne, M.; Behm, R. J. *J. Catal.* **2006**, *244*, 137−152.
(10) Guan, Y. J.; Ligthart, D. A. J. M.; Pirgon-Galin, O.; Pieterse, J. A. Z.; van Santen, R. A.; Hensen, E. J. M. *Top. Catal.* **2011**, *54*, 424−438.
(11) Guan, Y. J.; Hensen, E. J. M. *Phys. Chem. Chem. Phys.* **2009**, *11*, 9578−9582.
(12) Si, R.; Tao, J.; Evans, J.; Park, J. B.; Barrio, L.; Hanson, J. C.; Zhu, Y. M.; Hrbek, J.; Rodriguez, J. A. *J. Phys. Chem. C* **2012**, *116*, 23547−23555.
(13) Wang, X.; Rodriguez, J. A.; Hanson, J. C.; Perez, M.; Evans, J. *J. Chem. Phys.* **2005**, *123*, 221101.
(14) Wang, J.; Kisperky, V. F.; Delgass, W. N.; Ribeiro, F. H. *J. Catal.* **2012**, *289*, 171−178.
(15) Williams, W. D.; Shkhar, M.; Lee, W. S.; Kispersky, V.; Delgass, W. N.; Ribeiro, F. H.; Kim, S. M.; Stach, E. A.; Miller, J. T.; Allard, L. F. *J. Am. Chem. Soc.* **2010**, *132*, 14018−14020.
(16) Shekhar, M.; Wang, J.; Lee, W. S.; Akatay, M. C.; Stach, E. A.; Delgass, W. N.; Ribeiro, F. H. *J. Catal.* **2012**, *293*, 94−102.

(17) Shido, T.; Iwasawa, Y. *J. Catal.* **1992**, *136*, 493−503.
(18) Shido, T.; Iwasawa, Y. *J. Catal.* **1993**, *141*, 71−81.
(19) (a) Jacobs, G.; Williams, L.; Graham, U.; Thomas, G. A.; Sparks, D. E.; Davis, B. H. *Appl. Catal., A* **2003**, *252*, 107−118. (b) Jacobs, G.; Patterson, P. M.; Sparks, D. E.; Davis, B. H. *Appl. Catal., A* **2004**, *269*, 63−73. (c) Jacobs, G.; Khalid, S.; Patterson, P. M.; Sparks, D. E.; Davis, B. H. *Appl. Catal., A* **2004**, *268*, 255−266. (d) Jacobs, G.; Chenu, E.; Patterson, P. M.; Williams, L.; Sparks, D.; Thomas, G.; Davis, B. H. *Appl. Catal., A* **2004**, *258*, 203−214.
(20) Meunier, F. C.; Reid, D.; Goguest, A.; Shekhtman, S.; Hardacre, C.; Burch, R.; Deng, W.; Flytzani-Stephanopoulos, M. *J. Catal.* **2007**, *247*, 277−287.
(21) Liu, Z. P.; Jenkins, S. J.; King, D. A. *Phys. Rev. Lett.* **2005**, *94*, 4.
(22) Rodriguez, J. A.; Liu, P.; Hrbek, H.; Evans, J.; Perez, M. *Angew. Chem., Int. Ed.* **2007**, *46*, 1329−1332.
(23) Rodriguez, J. A.; Hanson, J. C.; Stacchiola, D.; Senanayake, S. D. *Phys. Chem. Chem. Phys.* **2013**, *15*, 12004−12025.
(24) Gokhale, A. A.; Dumestic, J. A.; Mavrikakis, M. *J. Am. Chem. Soc.* **2008**, *130*, 1402−1414.
(25) Liu, X. M.; Ni, Z. M.; Yao, P.; Xu, Q.; Mao, J. H.; Wang, Q. Q. *Acta Phys.−Chim. Sin.* **2010**, *26*, 1599−1606.
(26) Chen, Y.; Cheng, J.; Hu, P.; Wang, H. F. *Surf. Sci.* **2008**, *602*, 2828−2834.
(27) Chen, Y.; Wang, H. F.; Burch, R.; Hardacre, C.; Hu, P. *Faraday Discuss.* **2011**, *152*, 121−133.
(28) Si, R.; Flytzani-Stephanopoulos, M. *Angew. Chem., Int. Ed.* **2008**, *47*, 2884−2887.
(29) Zhou, K. B.; Wang, X.; Sun, X. M.; Peng, Q.; Li, Y. D. *J. Catal.* **2005**, *229*, 206−212.
(30) Du, X.; Zhang, D.; Shi, L.; Gao, R.; Zhang, J. *J. Phys. Chem. C* **2012**, *116*, 10009−10016.
(31) (a) Hsiao, W. I.; Lin, Y. S.; Chen, Y. C.; Lee, C. S. *Chem. Phys. Lett.* **2007**, *441*, 294−299. (b) Chowdhury, S.; Lin, K.-S. *J. Nanomater.* **2011**, *2011*, 1−16.
(32) (a) Aneggi, E.; de Leitenburg, C.; Llorca, J.; Trovarelli, A. *Catal. Today* **2012**, *197*, 119−126. (b) Aneggi, E.; Wiater, D.; de Leitenburg, C.; Liorca, J.; Trovarelli, A. *ACS. Catal.* **2014**, *4*, 172−181.
(33) Song, W. Y.; Hensen, E. J. M. *J. Phys. Chem. C* **2013**, *117*, 7721−7726.
(34) Song, W. Y.; Hensen, E. J. M. *Catal. Sci. Technol.* **2013**, *3*, 3020−3029.
(35) Song, W. Y.; Jansen, A. P. J.; Hensen, E. J. M. *Faraday Discuss.* **2013**, *162*, 281−293.
(36) Perdew, J. P.; Burke, K.; Ernzerhof, M. *Phys. Rev. Lett.* **1996**, *77*, 3865−3868.
(37) Kresse, G.; Furthmuller, J. *Comput. Mater. Sci.* **1996**, *6*, 15−50.
(38) Kresse, G.; Furthmuller, J. *Phys. Rev. B* **1996**, *54*, 11169−11186.
(39) Kresse, G.; Hafner, J. *Phys. Rev. B* **1993**, *47*, 558−561.
(40) Dudarev, S. L.; Botton, G. A.; Savrasov, S. Y.; Humphreys, C. J.; Sutton, A. P. *Phys. Rev. B* **1998**, *57*, 1505−1509.
(41) Blöchl, P. E. *Phys. Rev. B* **1994**, *50*, 17953−17979.
(42) Kresse, G.; Jouber, D. *Phys. Rev. B* **1999**, *59*, 1758−1775.
(43) Bengone, O.; Alouani, M.; Blöchl, P. E.; Hugel, J. *Phys. Rev. B* **2000**, *62*, 16392−16401.
(44) Fabris, S.; de Gironcoli, S.; Baroni, S.; Vicario, G.; Balducci, G. *Phys. Rev. B* **2005**, *72*, 237102.
(45) Cococcioni, M.; de Gironcoli, S. *Phys. Rev. B* **2005**, *71*, 035105.
(46) Castleton, C. W.; Kullgren, J.; Hermansson, K. *J. Chem. Phys.* **2007**, *127*, 244704.
(47) (a) Zhang, C. J.; Michaelides, A.; King, D. A.; Jenkis, S. J. *J. Chem. Phys.* **2008**, *129*, 194708. (b) Zhang, C. J.; Michaelides, A.; King, D. A.; Jenkis, S. J. *J. Phys. Chem. C* **2009**, *113*, 6411−6417.
(48) Da Silva, J.; Ganduglia-Pirovano, M.; Sauer, J.; Bayer, V.; Kresse, G. *Phys. Rev. B* **2005**, *75*, 045121.
(49) Henkelman, G.; Uberuaga, B. P.; Jonsson, H. *J. Chem. Phys.* **2000**, *113*, 9901−9904.
(50) (a) Green, I. X.; Tang, W.; Neurock, M.; Yates, J. T. *Science* **2011**, *333*, 736−739. (b) Molina, L. M.; Hammer, B. *Phys. Rev. B* **2004**, *69*, 155424. (b) Molina, L. M.; Rasmussen, M. D.; Hammer, B. *J. Chem. Phys.* **2004**, *120*, 7673−7680.
(51) Kumar, S.; Schelling, P. K. *J. Chem. Phys.* **2006**, *125*, 204704.
(52) (a) Rodriguez, J. A. *Catal. Today* **2010**, *160*, 3−10. (b) Mudiyanselage, K.; Senanayake, S. D.; Feria, L.; Kundu, S.; Baber, A. E.; Graciani, J.; Vidal, A. B.; Agnoli, S.; Evans, J.; Chang, R.; Axnanda, S.; Liu, Z.; Sanz, J. F.; Liu, P.; Rodriguez, J. A.; Stacchiola, D. J. *Angew. Chem., Int. Ed.* **2013**, *52*, 5101−5105.
(53) (a) Zhang, C.; Michaelides, A.; King, D. A.; Jenkins, S. J. *J. Am. Chem. Soc.* **2010**, *132*, 2175−2182. (b) Ghosh, P.; Camellone, M. F.; Fabris, S. *J. Phys. Chem. Lett.* **2013**, *4*, 2256−2263.
(54) Tabakova, T.; Boccuzzi, F.; Manzoli, M.; Sobczak, J. W.; Idakiev, V.; Andreeva, D. *Appl. Catal., B* **2004**, *49*, 73−81.
(55) Camellone, M. F.; Fabris, S. *J. Am. Chem. Soc.* **2009**, *131*, 10473−10483.
(56) Kim, H. Y.; Lee, H. M.; Henkelman, G. *J. Am. Chem. Soc.* **2012**, *134*, 1560−1570.
(57) Guzman, J.; Carrettin, S.; Corma, A. *J. Am. Chem. Soc.* **2005**, *127*, 3286−3287.
(58) Huang, X.; Sun, H.; Wang, L.; Liu, Y.; Fan, K.; Cao, Y. *Appl. Catal., B* **2009**, *90*, 224−232.
(59) Agarwal, S.; Lefferts, L.; Mojet, B. L. *ChemCatChem* **2013**, *5*, 479−489.
(60) Agarwal, S.; Lefferts, L.; Mojet, B. L.; Ligthart, D. A. J.; Hensen, E. J. M.; Mitchell, D. R. G.; Erasmus, W. J.; Anderson, B. G.; Olivier, E. J.; Neethling, J. H.; Datye, A. K. *ChemSusChem* **2013**, *6*, 1898−1906.